


RESEARCH

Open Access



# Bond Properties of CFRP Externally Bonded Reinforcement on Groove in Concrete

Zehong Han<sup>1</sup>, Jing Gao<sup>1\*</sup> , Huaihui Song<sup>1</sup> and Gongyi Xu<sup>2</sup>

## Abstract

Externally bonded reinforcement on groove (EBROG) is a significant reinforcement technology proposed by researchers to enhance the bond properties of reinforced concrete structural members. To understand the influence of groove size on concrete specimens of different strength, a total of 60 concrete specimens with 4 different strengths were cast with the single shear test in this paper, among which 48 EBROG specimens and 12 specimens with externally bonded reinforcement method (EBR) were used as the control group. The failure modes and failure mechanisms of specimens with various sizes and reinforcement methods were analyzed. Additionally, the test results of ultimate load, load–displacement curves, and bond-slip curves for specimens with different groove sizes were compared. The effectiveness of EBROG method in enhancing the ultimate load capacity at the bond interface of the specimens is proved. Furthermore, in situations where the volume of the groove was kept constant, the specimens with lower concrete strength and deeper groove exhibited superior bond properties. Also, the influence of groove width on bond properties was better than that of groove depth. Finally, the test results in this paper were compared with the prediction of the existing EBR and EBROG models to evaluate the performance of different models, and based on the original model, a prediction model for EBROG method in the groove region with higher accuracy was proposed.

**Keywords** CFRP sheets, Concrete strength grade, Groove size, EBROG, Bond properties

## 1 Introduction

Fiber reinforced polymer (FRP) composites have been utilized extensively in strengthening concrete structures due to their advantageous properties, such as high tensile strength and corrosion resistance (Li et al., 2022; Massou et al., 2023; Tatar & Milev, 2021; Teng & Smith, 2002). The bond properties of FRP-to-concrete are a crucial factor that determines the effectiveness of concrete reinforcement (Aram et al., 2008; Chen & Teng, 2001; Lu et al., 2005). A traditional method,

externally bonded reinforcement (EBR), often experienced premature debonding before the material reached its ultimate strength (Amirreza & Davood, 2018; Teng et al., 2003). Externally bonded reinforcement on groove (EBROG) and externally bonded reinforcement in groove (EBRIG) had been introduced for concrete reinforcement to enhance the bond properties between the FRP sheet and concrete (Mostofinejad & Mahmoudabadi, 2010; Mostofinejad & Shameli, 2013; Reza & Davood, 2022). EBROG was effective in strengthening concrete specimens and preventing debonding failures had been proved (Hosseini & Mostofinejad, 2013a; Khaled et al., 2022; Riyam et al., 2021). It had been observed that the groove width had great effect on improving the bonding stiffness and interfacial fracture energy was increased by increasing the groove depth (Hosseini & Mostofinejad, 2013b). The increase in groove depth enhanced the bond strength, and deeper groove was more effective for low-strength

Journal information: ISSN 1976-0485 / eISSN 2234-1315.

\*Correspondence:

Jing Gao

gaojing@xmu.edu.cn

<sup>1</sup> School of Architecture and Civil Engineering, Xiamen University, Xiamen 361005, Fujian, China

<sup>2</sup> China Railway Bridge Survey and Design Institute Group Co. LTD, Hubei 430050, Wuhan, China

concrete (Mostofinejad et al., 2018). Moreover, for a given groove width, a remarkable improvement on bond properties can be achieved by an optimal groove depth in EBROG method (Amir & Niloufar, 2019a, 2019b; Shaofei et al., 2023; Zolfaghari et al., 2023).

The shear stress distribution at the interface of concrete-FRP sheet plays a crucial role in determining the bond behavior of the FRP sheet. The transfer of tensile stress from the concrete specimen to FRP sheet is facilitated through the interfacial shear stress (Lu et al., 2005). To comprehend the relationship between the shear stress at the concrete-FRP sheet interface and the displacement of the composite material relative to the concrete surface, bilinear and nonlinear prediction models had been proposed based on test results. Dai et al. (2005) developed a bond-slip model for EBR reinforced concrete members, which was more accurate in predicting the bond properties of EBR reinforced specimens. Teng et al. (Aram et al., 2008; Teng et al., 2006) adopted a bilinear bond-slip model to analyze the whole process of interfacial bond-slip behavior in EBR reinforced concrete. Wang et al. () used a nonlinear bond-slip model to simulate the shear stress-slip relationship at the interface of concrete specimens reinforced by EBR, which was verified by test results. Fathi et al. (2023) proposed a bilinear bond-slip model based on the width factor obtained from the model in the literature (Lin et al., 2017). However, traditional EBR models don't accurately predict the bond-slip relationship of EBROG reinforced concrete. Consequently, Mofrada et al. (2019) proposed a nonlinear bond-slip model that exhibits high precision and is suitable for predicting the bond behavior and strength of EBR and EBROG methods. Moghaddas et al. (2021) proposed a bilinear bond-slip model based on their test results, which can predict bond strengths in 95% of the EBROG specimens with errors below 15% and applicable to concrete specimens reinforced by both the EBR and EBROG methods.

The existing researches had highlighted the significant influence of groove width and groove depth on the bond properties of EBROG specimens. Zolfaghari et al. (2023) emphasized the importance of finding the optimal combination of groove width and groove depth to achieve the best bond properties in EBROG reinforced specimens. However, few studies explored the effect of groove size on concrete specimens with different strength grades. To address this gap, the effect of groove width and groove depth on the bond properties of EBROG specimens with different concrete strength will be investigated in this paper through single shear tests. The test results were compared with the prediction of the existing EBR and EBROG models to evaluate the performance of different models. Furthermore, a new prediction model for

EBROG method with high accuracy, based on the original model, was proposed to predict the maximum shear stress on the groove.

## 2 Experimental Procedure

### 2.1 Specimen Detail

A total of 60 specimens were prepared, including 12 specimens using EBR method and 48 specimens using EBROG method. The EBR specimens were served as the control group, while concrete strength, groove width and groove depth were critical parameters in the design of EBROG group. To ensure the integrity of the CFRP sheets and prevent any premature damage during test, two aluminum sheets, 150 mm×50 mm×1 mm, were used to fix the CFRP sheet on the loading end. The CFRP sheet was 50 mm wide and had a bond length of 200 mm. A 30 mm unbonded length was intentionally left at the end of all specimens to avoid shear failure caused by stress concentration during loading process (Wu et al., 2012; Yao et al., 2005). Due to the groove in the middle of the specimen by EBROG method, the strain gauges were divided into two distinct regions at regular intervals of 50 mm on the groove region, as shown in Fig. 1.

To ensure a clean and uniform surface for effective bonding, mechanical grinding tools and air gun nozzle were used to remove any loose or fragile material from the concrete surface. The groove in EBROG specimen was then fully filled with epoxy glue. Two layers of CFRP sheet were impregnated with epoxy adhesive and securely pasted onto the prepared concrete surface inside the groove. For EBR specimens, the concrete surface was mechanically ground to expose the coarse aggregate on a textured open surface. An epoxy primer was applied to the textured surface to enhance adhesion. The CFRP sheets were bonded to the concrete surface using an epoxy resin binder. All specimens were kept at room temperature for two weeks to complete the curing process. The specimen was labeled as "C30-5-10-1" corresponded to the first specimen with concrete strength grade C30, groove depth of 5 mm and groove width of 10 mm.

### 2.2 Material Properties

To achieve a strong and durable bond between CFRP sheets and concrete surface, an epoxy resin adhesive with outstanding properties was selected. The measured performance indicators of CFRP sheets and epoxy resin according to GB/T3354 (2014) and GB/T1447 (2005) are shown in Table 1. The mixture of four different strength according to JGJ 55 (2011) is demonstrated in Table 2.

### 2.3 Test Setup and Instrumentation

The WAW-2000 microcomputer-controlled electro hydraulic servo universal testing machine was

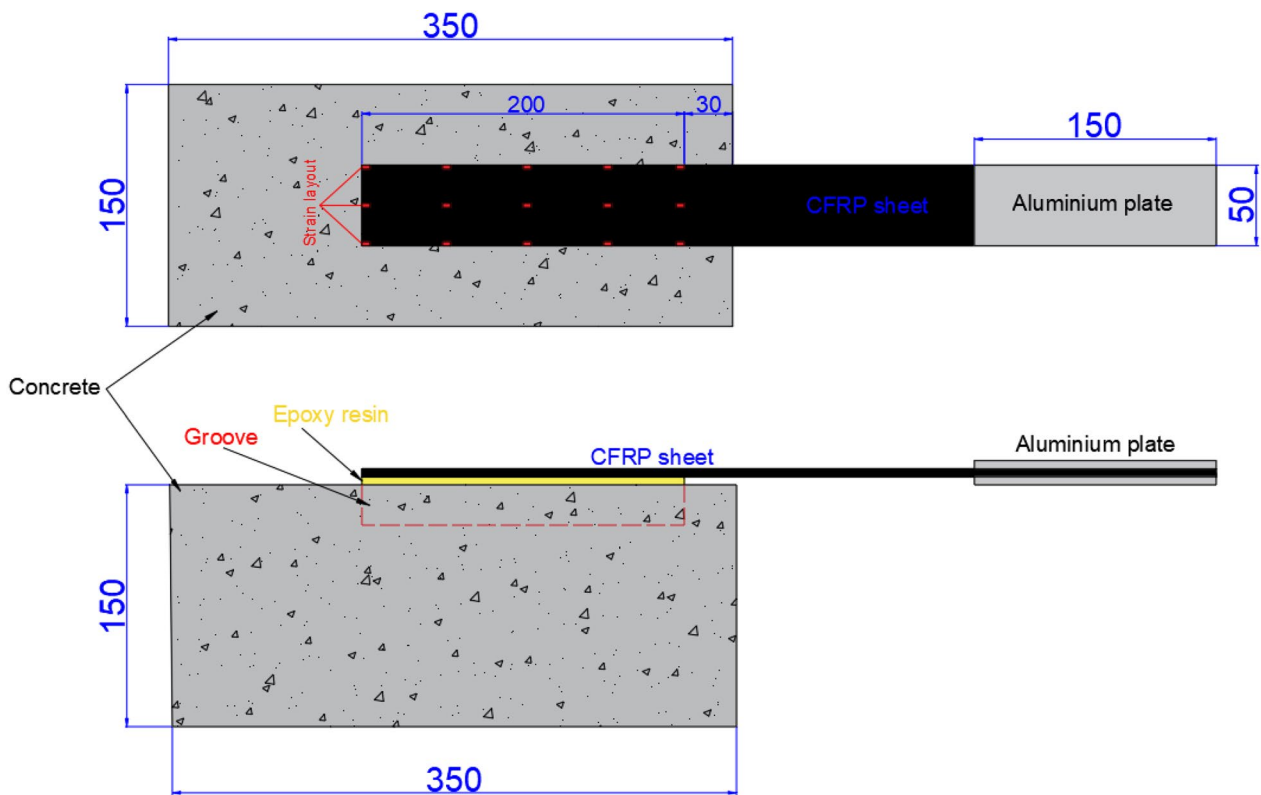


**Fig. 1** Configuration of the specimen

**Table 1** Material properties of CFRP sheets and Epoxy Resin

Material	Length (mm)	Width (mm)	Thickness (mm)	Elastic modulus (GPa)	Tensile strength (MPa)	Elongation %
CFRP sheet	550	50	0.167	231	3468	1.50
Epoxy resin	–	–	–	311	48.8	1.73

**Table 2** Details of concrete mixture [unit: kg/m<sup>3</sup>]

Strength grade	Water	Water reducer	Coal Ash	Cement	Fine aggregate	Coarse aggregate
C30	172.00	3.30	66.09	264.34	721.08	1176.49
C40	172.00	4.08	81.57	326.30	637.04	1183.08
C50	172.00	4.98	99.61	398.44	588.18	1141.76
C60	172.00	5.69	113.75	455.01	580.73	1078.50

employed in the test. To ensure loading stability and precision during test, a well-designed steel frame was utilized as shown in Fig. 2. The loading following specification ACI440.1R-06 (ACI440.1R-06, 2006). The loading rate was set at 0.5 mm/min. During the loading, the fixed screws at the top of the steel frame were

securely fixed into the testing setup. The CFRP sheets were connected to aluminum sheets fixed at the lower part of the test setup. The load, displacement and strain were continuously recorded in a strain collection system.

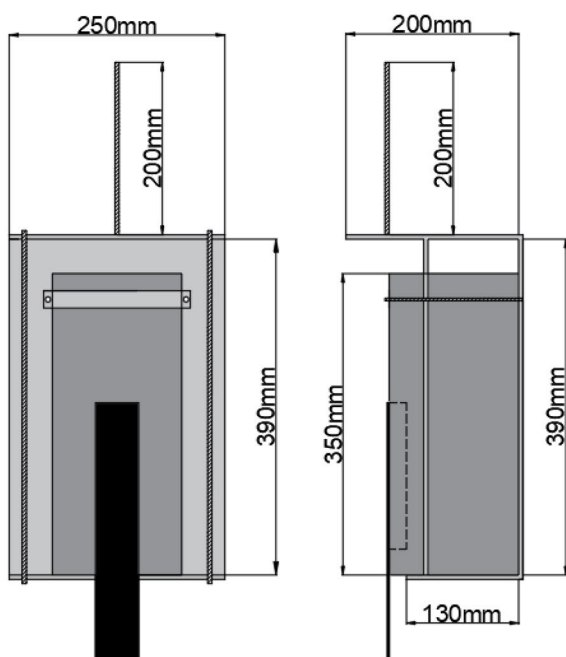


**Fig. 2** Steel frame for supporting concrete specimen

### 3 Analysis of Experimental Results

#### 3.1 Failure Modes and Ultimate Load

The results and failure modes obtained from the single shear test are provided in Table 3 and the main failure modes of each specimen are shown in Fig. 3.

There were three kinds of failure modes in the test, debonding failure, fracture failure of CFRP sheet, and composite failure, denoted by D, F and C respectively. It can be concluded from Table 3 that debonding failure is independent of concrete strength in all specimens with EBR method, in which the tensile strength of epoxy resin is significantly higher than that of concrete. Therefore, increase of concrete strength has no obvious effect on the improvement of bond properties in EBR specimens. In those specimens strengthened

with EBROG method, fracture failure of the CFRP sheet or composite failure occurred. However, concrete strength has little effect on the failure modes, instead of groove width, which increase the bond area between CFRP sheet and concrete, allowing for a more effective transfer of interfacial shear stress. Composite failure occurred when the bond strength is lower than the tensile strength of the CFRP sheet. While when the bond strength is higher than the tensile strength of the CFRP sheet, the fracture failure of CFRP sheet is dominated.

Table 3 shows the ultimate load of each specimen. It demonstrates that for each concrete strength, there is an optimum combination of groove sizes resulting in the maximum loading capacity for the EBROG specimens. Notably, at the same concrete strength grade, the ultimate load of EBROG specimens are above two times of EBR specimens, highlighting the remarkable strengthening effect of the EBROG method. Taking C40 group as an example, increasing of ultimate load compared with EBR specimens is shown in Fig. 4. It indicates that the optimum groove sizes, with a depth of 15 mm and width of 20 mm, can be achieved for C40 group when its ultimate load reaches the maximum. This suggests specific groove sizes should be chosen to achieve a best enhancement at specific concrete strength.

#### 3.2 The Effect of Groove Size

The influence of groove size on the ultimate load of EBROG specimens is shown in Fig. 5, where the letter “V” represents the volume of the groove. It indicates that the effect of groove size on the bond strength of the interface varies for EBROG specimens with different concrete strengths.

Increase in groove volume does not necessarily lead to a linear increase in the ultimate load of the specimens. Instead, the effect of groove volume on the ultimate load is closely related to the specific groove width and depth. Regardless of the concrete strength, when the groove volume is the same, the ultimate load of the specimen with a wider groove is larger, which indicates that groove width plays a more critical role in determining the bond strength and ultimate load of the EBROG specimens. For C40 group, when the groove volume is the same, the ultimate load value of the specimen with a deeper groove is larger. However, for C60 group, when the groove volume is the same, the ultimate load of the specimen with a deeper groove is smaller. It can be concluded that, for lower concrete strength, increasing the groove depth contributes to improving the bond strength and ultimate load of the EBROG specimens. Conversely, for higher concrete strength grades, a smaller groove depth can result in better bond strength and ultimate load for EBROG specimens.

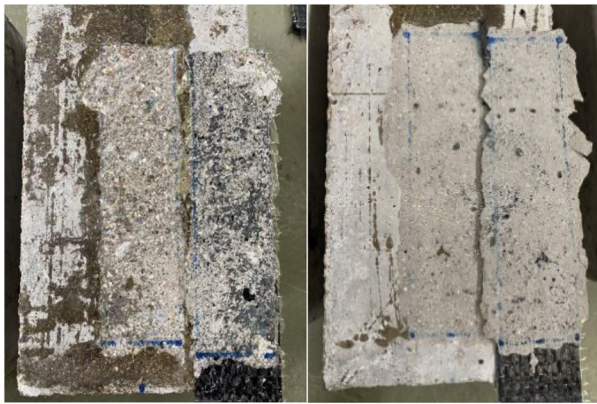
**Table 3** Experimental results and failure mode

Specimen-number	Concrete-strength (MPa)	Groove depth (mm)	Groove width (mm)	Groove volume (cm <sup>3</sup> )	Ultimate load (kN)	Average load (kN)	Failure mode
C30-0-0-1	38.3	–	–	–	7.00	6.83	D
C30-0-0-2	38.3	–	–	–	6.01		D
C30-0-0-3	38.3	–	–	–	7.49		D
C30-5-5-1	38.3	5	5	5	9.16	9.62	C
C30-5-5-2	38.3	5	5	5	10.30		F
C30-5-5-3	38.3	5	5	5	9.39		C
C30-10-10-1	38.3	10	10	20	13.31	11.80	F
C30-10-10-2	38.3	10	10	20	11.04		C
C30-10-10-3	38.3	10	10	20	11.05		F
C30-15-15-1	38.3	15	15	45	14.12	13.63	F
C30-15-15-2	38.3	15	15	45	13.39		C
C30-15-15-3	38.3	15	15	45	13.93		F
C30-20-20-1	38.3	20	20	80	18.93	18.96	C
C30-20-20-2	38.3	20	20	80	19.07		F
C30-20-20-3	38.3	20	20	80	18.87		C
C40-0-0-1	48.0	–	–	–	8.61	7.93	D
C40-0-0-2	48.0	–	–	–	8.13		D
C40-0-0-3	48.0	–	–	–	7.05		D
C40-5-10-1	48.0	5	10	10	12.14	13.42	F
C40-5-10-2	48.0	5	10	10	14.61		C
C40-5-10-3	48.0	5	10	10	13.52		C
C40-10-5-1	48.0	10	5	10	12.07	13.07	F
C40-10-5-2	48.0	10	5	10	12.76		F
C40-10-5-3	48.0	10	5	10	14.38		F
C40-15-20-1	48.0	15	20	60	16.50	17.05	F
C40-15-20-2	48.0	15	20	60	18.07		C
C40-15-20-3	48.0	15	20	60	16.57		F
C40-20-15-1	48.0	20	15	60	13.84	12.54	F
C40-20-15-2	48.0	20	15	60	10.19		C
C40-20-15-3	48.0	20	15	60	13.61		F
C50-0-0-1	53.7	–	–	–	6.09	7.44	D
C50-0-0-2	53.7	–	–	–	8.35		D
C50-0-0-3	53.7	–	–	–	7.87		D
C50-5-15-1	53.7	5	15	15	16.49	15.22	F
C50-5-15-2	53.7	5	15	15	14.55		C
C50-5-15-3	53.7	5	15	15	14.63		F
C50-10-20-1	53.7	10	20	20	18.49	17.73	C
C50-10-20-2	53.7	10	20	20	18.62		F
C50-10-20-3	53.7	10	20	20	16.09		C
C50-15-5-1	53.7	15	5	15	11.08	10.68	F
C50-15-5-2	53.7	15	5	15	10.35		C
C50-15-5-3	53.7	15	5	15	10.61		F
C50-20-10-1	53.7	20	10	40	14.81	13.64	F
C50-20-10-2	53.7	20	10	40	13.83		C
C50-20-10-3	53.7	20	10	40	12.29		C
C60-0-0-1	65.6	–	–	–	6.70	6.85	D
C60-0-0-2	65.6	–	–	–	7.19		D
C60-0-0-3	65.6	–	–	–	6.65		D



**Table 3** (continued)

Specimen-number	Concrete-strength (MPa)	Groove depth (mm)	Groove width (mm)	Groove volume (cm <sup>3</sup> )	Ultimate load (kN)	Average load (kN)	Failure mode
C60-5-20-1	65.6	5	20	20	16.30	15.68	C
C60-5-20-2	65.6	5	20	20	14.91		C
C60-5-20-3	65.6	5	20	20	15.84		C
C60-10-15-1	65.6	10	15	30	13.83	13.91	C
C60-10-15-2	65.6	10	15	30	14.38		C
C60-10-15-3	65.6	10	15	30	13.52		F
C60-15-10-1	65.6	15	10	30	13.37	12.52	F
C60-15-10-2	65.6	15	10	30	13.33		C
C60-15-10-3	65.6	15	10	30	10.87		C
C60-20-5-1	65.6	20	5	20	10.29	11.18	C
C60-20-5-2	65.6	20	5	20	11.64		F
C60-20-5-3	65.6	20	5	20	11.61		C



(a)



(b)



(c)

**Fig. 3** Failure modes of specimens (a Debonding failure, b CFRP sheets fracture failure, c Composite failure)

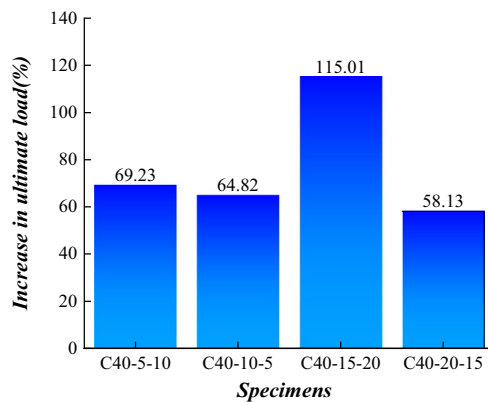


**Fig. 4** Increase in ultimate load of EBROG compared to EBR

### 3.3 Load–Displacement Behavior

The load–displacement curves of C40 and C50 groups are drawn, as shown in Fig. 6. The three stages observed in the load–displacement curves, namely the elastic stage, softening stage, and failure stage. At the initial stage of loading, the load and displacement exhibit a linear increase, indicating that the bond interface between the CFRP sheets and concrete is in elastic stage. As the load continued to increase and approaches 85% of the ultimate load, the curve enters the softening stage. In this stage, the bond interface between CFRP sheets and the concrete begins to weaken, leading to a gradual loss of bond strength. As a result, the slope of the load–displacement curve becomes smaller as the specimen starts to experience debonding or separation between the CFRP sheets and the concrete. In failure stage, with the expansion of microcracks at the concrete surface, the adhesive layer between the CFRP sheets and the concrete was destroyed, CFRP was completely separated from the concrete under the failure load (Yuan et al., 2019), then brittle damage occurred abruptly.

Energy absorption ability is an important parameter to evaluate the ability of a specimen against non-elastic deformation and loading capacity. The area under the load–displacement curve is normally used to define the energy absorption capacity of the specimen (Gulec, 2023; Gulec et al., 2020, 2021), which is calculated by the following formula (Gulec et al., 2021):

$$\text{Energy absorption} = 0.5 \times (d_2 - d_1) \times (F_2 - F_1) \tag{1}$$

where  $d_1$  and  $d_2$  are two successive displacement points of the load–displacement curve;  $F$  is the load at this displacement;

The energy absorption capacity of the specimens is given in Table 4. Fig. 7 shows the increase in energy absorption of EBROG specimens compared with EBR specimens. It can be seen that the energy absorption

capacity of EBROG specimens is more than 100% higher compared to EBR specimens. Moreover, the specimen with a wider groove has a greater energy absorption capacity compared to the specimen with a deeper groove when the energy absorption capacities of the specimens with the same concrete strength were compared. It is clear that groove width had a better effect on improving the bond properties and loading capacity of specimens than groove depth.

### 3.4 Bond-slip Behavior

The bond-slip curve is an effective reference for evaluating the local bond properties of the bond interface, and it defines the constitutive relationship of bond properties between different materials. Up to now, many tests and studies on the bond-slip behavior of EBR reinforced specimens had been conducted (Al-Mahaidi & Kalfat, 2011; Dai et al., 2005; Teng et al., 2006; Wang, 2006a; Zhang, 2018; Zhou et al., 2010). But there were few studies on the bond-slip behavior of EBROG reinforced specimens, which will be analyzed in the section.

The interface shear stress can be calculated by the following formula (Al-Mahaidi & Kalfat, 2011):

$$\tau = \frac{E_f t_f (\varepsilon_{i+1} - \varepsilon_i)}{\Delta x} \tag{2}$$

where  $\tau$  is the shear stress between two consecutive measuring points;  $E_f$  is the elastic modulus of CFRP sheet;  $t_f$  is the thickness of CFRP sheet;  $\varepsilon_i$  and  $\varepsilon_{i+1}$  are the strain value at two consecutive measuring points;  $\Delta x$  is the distance between two measuring points.

The local slip between the concrete interface and the CFRP sheet is caused by the strain difference. When the bond length between the CFRP sheets and the concrete interface is long, it can be assumed that the slip at the free end is close to zero (Zhou et al., 2010). Therefore, the slippage of the bonding interface can be calculated by the following formula:

$$s_i = \frac{\Delta x}{2} \left( \varepsilon_0 + 2 \sum_j^{i-1} \varepsilon_j + \varepsilon_i \right) \tag{3}$$

where  $\varepsilon_i$  is the slippage of the measuring point  $i$ ;  $\varepsilon_0$  is the strain value of the first measuring point near the free end.

The bond-slip curves of C40 group are taken as an example to analyze the bond-slip behavior of EBR and EBROG specimens, which are shown in Fig. 8. It shows that both the bond-slip curves of EBR and EBROG specimens can be approximated by bilinear curves. These curves can be divided into two stages: the elastic deformation stage and the interface failure stage. In the elastic deformation stage, the bond behavior is relatively

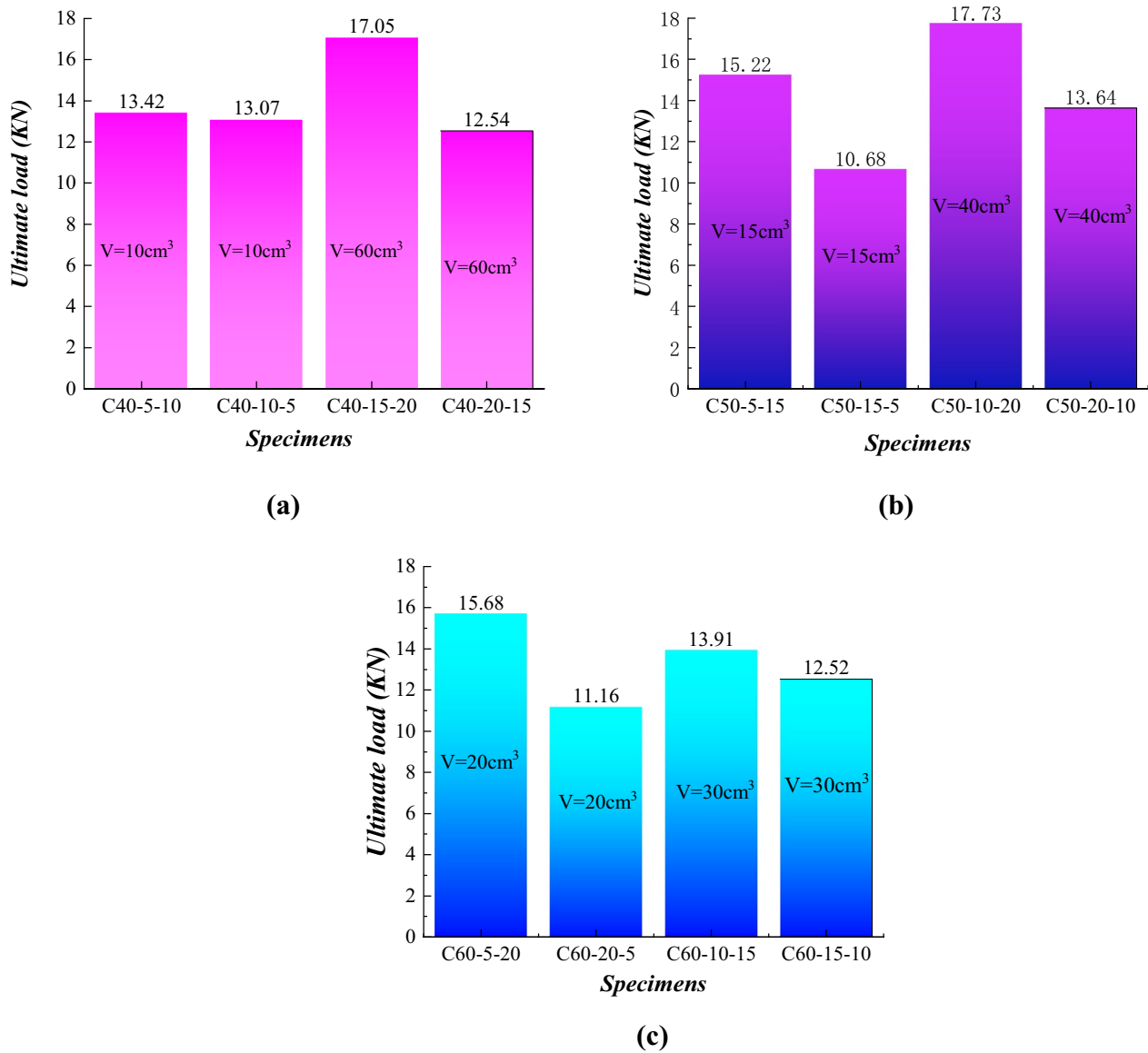


**Fig. 5** The effect of groove size on ultimate load (a C40 concrete specimen group, b C50 concrete specimen group, c C60 concrete specimen group)

linear, and the bond strength between the CFRP sheets and the concrete surface increases with increasing slip at the bond interface. The interface failure stage occurs when the bond strength reaches its maximum and starts to decrease as the slip continues to increase. At this stage, microcracks may develop at the FRP-concrete interface, leading to a reduction in the bond strength. Ultimately, debonding occurs, and the bond between the CFRP sheets and the concrete is lost.

The interfacial fracture energy is one of the key parameters affecting the debonding failure. It can be defined as the area under the bond-slip curve. When the bond

interface can withstand higher interfacial fracture energy, it proves that the bond strength is higher (Lin et al., 2017). The analysis of Fig. 8a and b highlights the difference in the bond-slip behavior between the outside-groove region and the groove region of EBROG specimens compared to EBR specimens. In the outside-groove region, the bond-slip behavior of EBROG specimens shows minimal improvement in terms of the maximum shear stress, interfacial fracture energy, and corresponding slip compared to EBR specimens.

However, in the groove region, the maximum shear stress and interfacial fracture energy are greatly increased



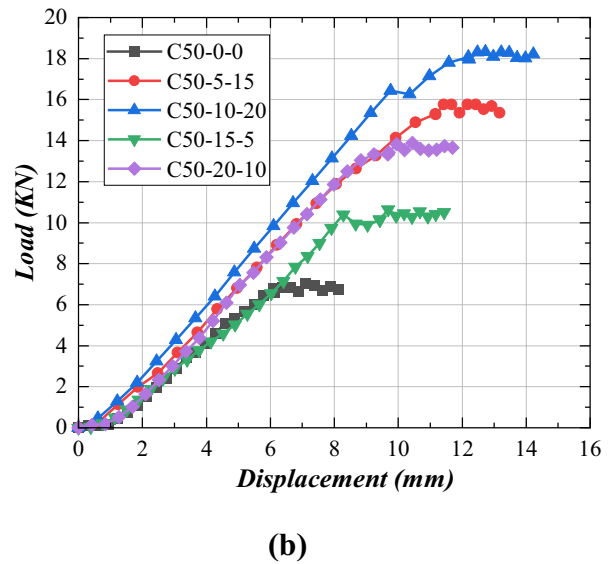
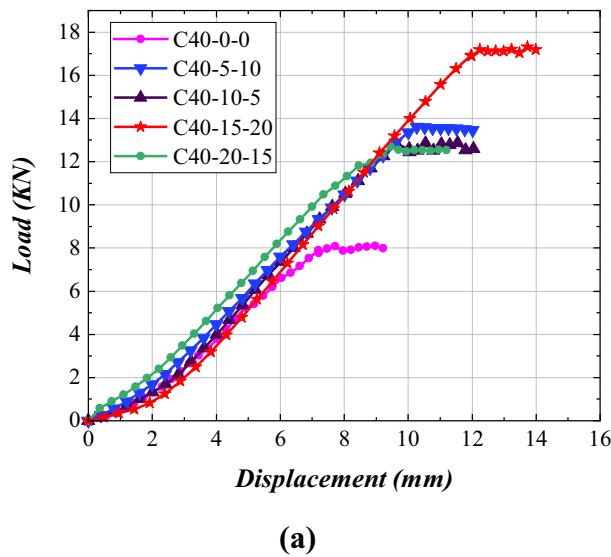


**Fig. 6** Load–displacement curves (a C40 specimens, b C50 specimens)

**Table 4** Energy absorption of EBROG and EBR specimens

Concrete strength	Specimen	Energy absorption (kN-mm)	Energy absorption ratio (EBROG/EBR)
C30	C30-0-0	17.96	–
	C30-5-5	40.18	2.24
	C30-10-10	51.86	2.89
	C30-15-15	60.27	3.36
	C30-20-20	112.85	6.28
C40	C40-0-0	31.11	–
	C40-5-10	69.82	2.24
	C40-10-5	62.39	2.01
	C40-15-20	105.14	3.38
	C40-20-15	60.98	1.96
C50	C50-0-0	22.57	–
	C50-5-15	89.99	3.99
	C50-10-20	114.16	5.06
	C50-15-5	51.55	2.28
	C50-20-10	69.11	3.06
C60	C60-0-0	21.93	–
	C60-5-20	100.19	4.57
	C60-10-15	68.02	3.10
	C60-15-10	58.97	2.69
	C60-20-5	66.82	3.05

compared to EBR specimens which indicates that the presence of groove effectively enhances the bond strength and resistance to debonding. Furthermore, increasing the width of the groove results in a more significant

improvement in bond properties compared to increasing the depth of the groove, which indicates that the groove width has a more substantial influence on the shear stress and interfacial fracture energy than the groove depth in the groove region.

## 4 Performance Evaluation of Proposed Models

### 4.1 Performance Evaluation of Existing EBR Models

The prediction of some EBR models and the test results of this paper are shown in Table 5, which demonstrates that an increase in concrete strength has a positive correlation with the maximum shear stress of EBR specimens. As the concrete strength increases, the bond strength between the CFRP sheets and concrete surface tends to increase, resulting in higher maximum shear stress.

Various prediction models were developed by some researchers to estimate the maximum shear stress of EBR specimens, considering many factors such as concrete strength, interfacial fracture energy, and the stiffness of the carbon fiber sheet. Among these models, the prediction model proposed by Dai et al. (2005) stood out as being relatively accurate in its predictions, matching the test results. In contrast, other prediction models proposed by Lu et al. (2005) and Sun et al. (2017) tended to overestimate the influence of concrete strength, leading to lower prediction accuracy. Moreover, the test results indicate that the maximum shear stress of EBR specimens is similar with EBROG specimens on the outside-groove region, and it is not significantly affected by the groove size. It suggests that the presence of groove in the

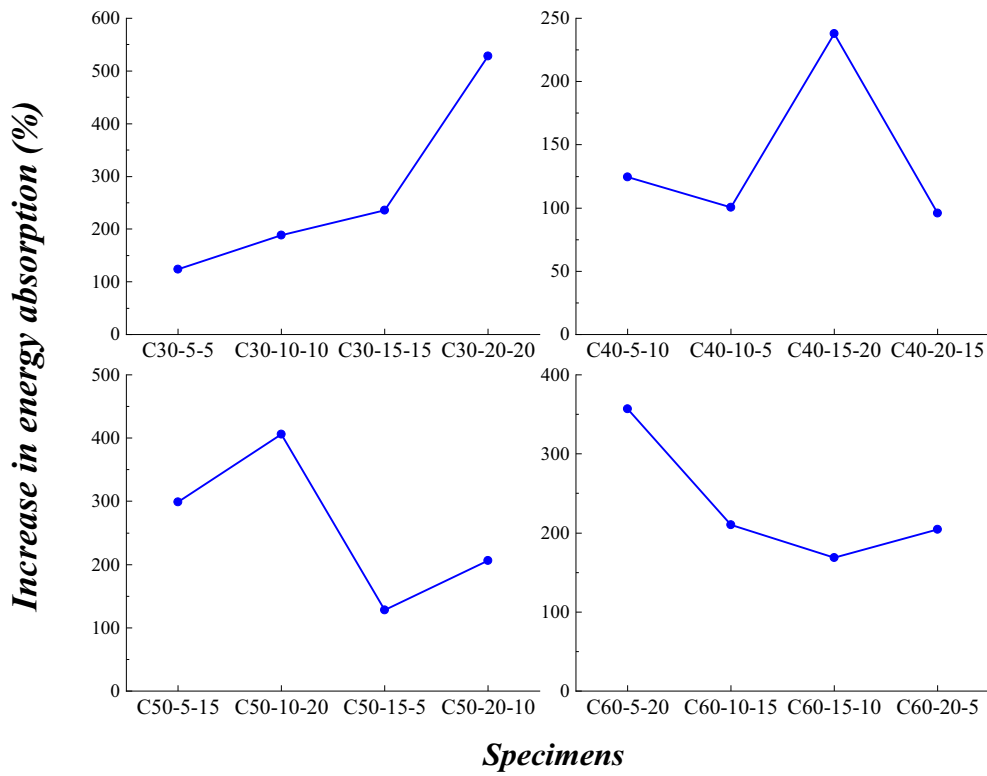


**Fig. 7** Increase in energy absorption of EBROG specimens compared to EBR specimens

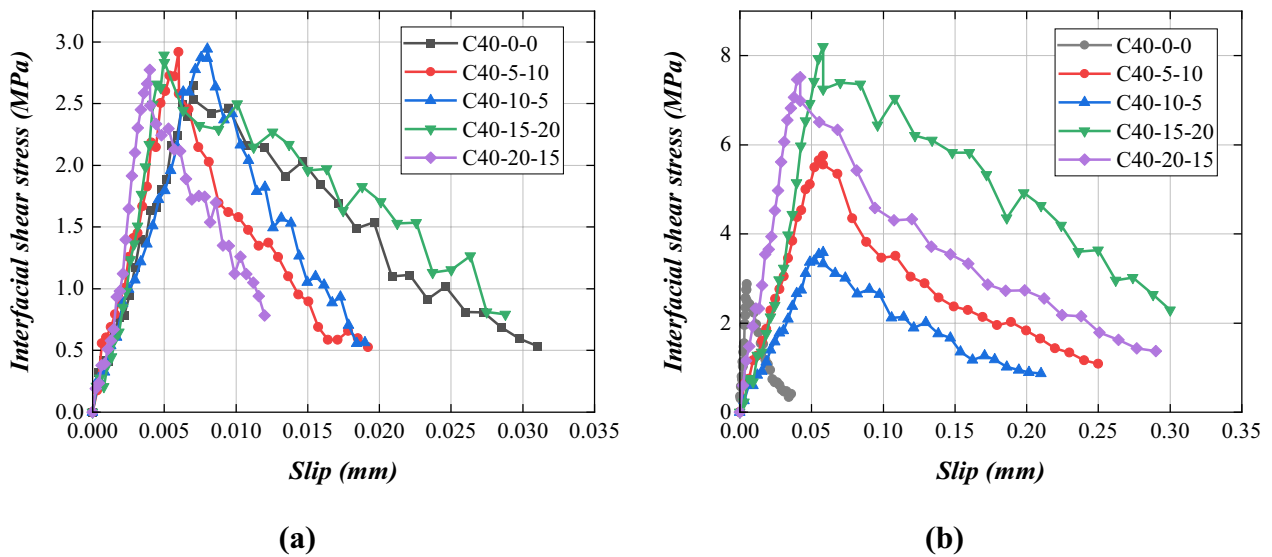


**Fig. 8** Bond-slip curves of C40 specimens (a outside-groove region; b groove region)

EBROG method does not significantly influence the maximum shear stress on the outside-groove region. Therefore, Dai’s model proves to be a better prediction model

for both EBR and EBROG specimens on the outside-groove region.

**Table 5** Maximum shear stress of specimens, along with the predictions of existing EBR models [unit: MPa]

Specimen number	This paper	Dai et al. (2023)	Lu et al. (2005)	Sun et al. (2017)
C30-0-0	2.71	3.69	4.24	4.81
C40-0-0	2.85	3.89	4.94	5.22
C50-0-0	3.08	3.99	5.22	5.45
C60-0-0	3.10	4.18	6.02	5.88

**4.2 Performance Evaluation of Existing EBROG Models**

As can be seen from Fig. 8, the bond-slip curves of EBROG specimens can be simplified into bilinear. Moghaddas et al. (2021), using test results, proposed a bilinear bond-slip model to predict the bond properties in outside-groove and groove region. The performance of Moghaddas’s model (Moghaddas et al., 2021) in predicting the maximum shear stress of EBROG specimens is compared with the test results of this paper in Table 6. The model accuracy can be calculated by the following formula:

$$\text{Model accuracy} = 100 - \frac{|\text{Experiment} - \text{Prediction}|}{\text{Experiment}} \times 100 \tag{4}$$

The analysis presented in Table 6 indicates that the model accuracy for predicting the maximum shear stress in the outside-groove region is less than 50%. It is observed that for specimens with smaller groove width, the predictions of the maximum shear stress in the groove position were

larger than the actual test results. This discrepancy may be attributed to the fact that the existing models overlooked the influence of groove width on the bond properties.

**4.3 Modification of the Existing Model**

Considering the influence of groove width on the bond properties of EBROG specimens is crucial for accurately predicting the maximum shear stress in the groove region. By modifying the calculation model proposed by Moghaddas et al. (2021), the maximum shear stress in the groove region is calculated as following formula:

$$\tau_{\max} = 0.277 \times (E_f t_f)^{0.3} f_c^{0.12} h^{0.1} w^{0.43} \tag{5}$$

where  $E_f$  is the elastic modulus of CFRP sheet;  $t_f$  is the thickness of CFRP sheet;  $f_c$  is the concrete compressive strength;  $h$  is groove depth;  $w$  is groove width.

**Table 6** The performance evaluation of the existing model

Specimen number	Outside-groove region			Groove region		
	This paper (MPa)	Moghaddas et al. (2021) (MPa)	Model accuracy (%)	This paper (MPa)	Moghaddas et al. (2021) (MPa)	Model accuracy (%)
C30-5-5	2.78	4.42	41.01	3.64	6.63	17.86
C30-10-10	2.79	4.74	30.11	4.42	7.11	39.14
C30-15-15	2.75	4.94	20.36	5.78	7.40	71.97
C30-20-20	2.76	5.08	15.94	8.11	7.62	93.96
C40-5-10	2.78	4.68	31.65	5.26	6.81	70.53
C40-10-5	2.89	5.01	26.64	3.76	7.30	5.85
C40-15-20	2.84	5.22	16.20	8.10	7.61	93.95
C40-20-15	2.84	5.37	10.92	7.16	7.83	90.64
C50-5-15	3.18	4.77	50.00	6.02	6.91	85.22
C50-10-20	2.95	5.11	26.78	7.42	7.40	99.73
C50-15-5	3.02	5.32	76.16	4.60	7.71	32.39
C50-20-10	3.04	5.48	19.74	5.24	7.93	48.66
C60-5-20	3.06	4.99	36.93	7.03	7.07	99.43
C60-10-15	2.94	5.34	18.37	6.68	7.58	86.53
C60-15-10	3.06	5.57	17.97	5.67	7.90	60.67
C60-20-5	3.11	5.73	15.76	4.73	8.13	28.12

**Table 7** The performance evaluation of the proposed model

Specimen number	Concrete strength (MPa)	$E_f t_f$ (kN/mm)	Groove depth (mm)	Groove width (mm)	Average test results	Average predictions	Model accuracy
C30-5-5	38.3	77.145	5	5	3.64	3.65	99.73
C40-15-20	48.0	77.145	15	20	8.10	7.49	92.47
C50-5-15	53.7	77.145	5	15	6.02	6.03	99.83
C60-15-10	65.6	77.145	15	10	5.67	5.81	97.53
G-32 (Moghaddas et al., 2021)	28.1	25.3	10	10	3.68	3.61	98.10
G-34 (Moghaddas et al., 2021)	39.1	39.1	10	10	4.39	4.28	97.49
G-48 (Moghaddas et al., 2021)	37.0	12.9	15	10	3.50	3.24	92.57
G-58 (Moghaddas et al., 2021)	37.9	78.2	15	10	5.93	5.46	92.07

#### 4.4 Verification of the New Proposed Model

The proposed model is verified using some test results, which is shown in Table 7. The model accuracy is more than 90% that indicates the proposed model can be used to predict the maximum shear stress in the groove region with higher accuracy.

#### 5 Conclusions

In this paper, the effects of groove width and groove depth on the CFRP-concrete interface loading capacity and bond properties of concrete reinforced specimens with different strengths, using EBR method and EBROG method were studied through the single shear test, and the accuracy of the bond-slip models of the existing EBR method and EBROG method was evaluated compared with the test results. The following conclusions can be drawn:

- (1) Debonding failure occurred in all specimens strengthened by the EBR method whereas CFRP sheet fracture failure and composite failure occurred in the specimens treated with the EBROG method. This difference can be attributed to the presence of the groove, which increased the bonding area between CFRP sheet and concrete and enhanced the bond properties of the reinforced specimens.
- (2) The bond properties of specimens reinforced by EBROG method consistently exhibited better results with changes in groove width than groove depth. The increase of groove width can improve the ability of energy absorption and loading capacity of the specimens with EBROG method, so as to improve the bonding properties.
- (3) Specimens with low concrete strength and deeper groove displayed higher loading capacity with the same groove sectional area, while specimens with

high concrete strength and shallower groove exhibited enhanced loading capacity.

- (4) Comparing with EBR specimens, the EBROG specimens demonstrated a significant increase in bond properties in the groove region, while there was little improvement in the outside-groove region.
- (5) Dai's EBR bond-slip model can accurately predict the maximum shear stress of EBROG specimens in the outside-groove region, and the new EBROG bond-slip model obtained by modifying Moghaddas's model had higher accuracy in predicting the maximum shear stress in the groove region.

#### Abbreviations

EBROG	Externally bonded reinforcement on groove
EBR	Externally bonded reinforcement

#### Acknowledgements

Not applicable.

#### Author contributions

ZH and JG analyzed the test results and interpreted the superiority of EBROG method compared to EBR method, and were the major contributors in writing the manuscript. HS assisted in finishing the test. GX was responsible for reviewing the manuscript. All authors read and approved the final manuscript.

#### Funding

This project was supported by the National Natural Science Foundation of China (No. U2005216), Natural Science Foundation of Fujian Province (No. 2020J01010).

#### Availability of data and materials

The authors declare that the datasets used or analyzed during the current study are available from the corresponding author on reasonable request.

#### Declarations

#### Competing interests

The authors declare that they have no known competing financial interests or personal relationships that could have appeared to influence the work reported in this paper. This project was supported by the National Natural Science Foundation of China (No. U2005216), Natural Science Foundation of Fujian Province (No. 2020J01010).

Received: 11 January 2024 Accepted: 11 March 2024  
Published online: 03 June 2024

## References

- ACI440.1R-06. (2006). Guide for the Design and Construction of Structural Concrete Reinforced with FRP Bars. ACI Committee.
- Al-Mahaidi, R., & Kalfat, R. (2011). Investigation into CFRP laminate anchorage systems utilizing bi-directional fabric wraps. *Composite Structures*, 93(4), 1265–1274. <https://doi.org/10.1016/j.compstruct.2010.10.012>
- Amir, T. R., & Niloufar, M. (2019a). Bond mechanical of EBROG method using a single groove to attach CFRP sheets on concrete. *Construction and Building Materials*, 197, 693–704. <https://doi.org/10.1016/j.conbuildmat.2018.11.204>
- Amir, T. R., & Niloufar, M. (2019b). Effect of the EBROG method on strip-to-concrete bond behavior. *Construction and Building Materials*, 220, 701–711. <https://doi.org/10.1016/j.conbuildmat.2019.06.065>
- Amirreza, M., & Davood, M. (2018). Empirical FRP-concrete bond strength model for externally bonded reinforcement on grooves. *Journal of Composites for Construction*, 04018080, 1–13. [https://doi.org/10.1061/\(ASCE\)CC.1943-5614.0000992](https://doi.org/10.1061/(ASCE)CC.1943-5614.0000992)
- Aram, M. R., Czaderski, C., & Motavalli, M. (2008). Debonding failure modes of flexural FRP-strengthened RC beams. *Composite Part b: Engineering*, 39(5), 826–841. <https://doi.org/10.1016/j.compositesb.2007.10.006>
- Chen, J. F., & Teng, J. G. (2001). Anchorage strength models for FRP and steel plates bonded to concrete. *Journal of Structural Engineering*, 127(7), 784–791. [https://doi.org/10.1061/\(ASCE\)0733-9445\(2001\)127:7\(784\)](https://doi.org/10.1061/(ASCE)0733-9445(2001)127:7(784))
- Dai, J., Ueda, T., & Sato, Y. (2005). Development of the nonlinear bond-slip model of fiber-reinforced plastics sheet-concrete interfaces with a simple method. *Journal of Composites for Construction*, 9(1), 52–62. [https://doi.org/10.1061/\(ASCE\)1090-0268\(2005\)9:1\(52\)](https://doi.org/10.1061/(ASCE)1090-0268(2005)9:1(52))
- Fathi, A., El-Saikaly, G., & Chaallal, O. (2023). Experimental and analytical study of bond stress-slip behavior at the CFRP-to-concrete interface. *Journal of Composites for Construction*, 27(2), 04023009. <https://doi.org/10.1061/JCCOF2.CCENG-4074>
- GB/T1447. (2005). Fiber-reinforced plastics composites-Determination of tensile properties. China National Standards Law Administration Committee.
- GB/T3354. (2014). Test method for tensile properties of orientation fiber reinforced polymer matrix composite materials. China National Standards Law Administration Committee.
- Gulec, A. (2023). Investigation of the effect of different curing conditions on the mechanical performance of calcium aluminate cement concrete at elevated temperatures. *Construction and Building Materials*, 409(15), 133920. <https://doi.org/10.1016/j.conbuildmat.2023.133920>
- Gulec, A., Kose, M. M., & Gogus, M. T. (2020). An analysis of the usability of prefabricated cage-reinforced composite beams with self-compacting and lightweight concrete under flexural loads. *Construction and Building Materials*, 255(20), 119274. <https://doi.org/10.1016/j.conbuildmat.2020.119274>
- Gulec, A., Kose, M. M., & Gogus, M. T. (2021). Experimental investigation of flexural performance of T-section prefabricated cage reinforced beams with self-compacting concrete. *Structures*, 33, 2190–2197. <https://doi.org/10.1016/j.jistruc.2021.05.074>
- Hosseini, A., & Mostofinejad, D. (2013a). Experimental investigation into bond behavior of CFRP sheets attached to concrete using EBR and EBROG techniques. *Composites, Part b: Engineering*, 51, 130–139. <https://doi.org/10.1016/j.compositesb.2013.03.003>
- Hosseini, A., & Mostofinejad, D. (2013b). Effect of groove characteristics on CFRP-to-concrete bond behavior of EBROG joints: Experimental study using particle image velocimetry (PIV). *Construction and Building Materials*, 49, 364–373. <https://doi.org/10.1016/j.conbuildmat.2013.08.036>
- JGJ55. (2011). Specification for mix proportion design of ordinary concrete. Ministry of Housing and Urban-Rural Development of the People's Republic of China.
- Khaled, S., Azad, Y., Davood, M., & Christoph, C. (2022). Bond behavior of FRP composites attached to concrete using EBROG method: A state-of-the-art review. *Composite Structures*, 299(1), 116060. <https://doi.org/10.1016/j.compstruct.2022.116060>
- Li, J., Mai, Z., Xie, J., & Lu, Z. (2022). Durability of components of FRP-concrete bonded reinforcement systems exposed to chloride environments. *Composite Structures*, 279(114697), 1–19. <https://doi.org/10.1016/j.compstruct.2021.114697>
- Lin, J. P., Wu, Y. F., & Smith, S. T. (2017). Width factor for externally bonded FRP-to-concrete joints. *Construction and Building Materials*, 155, 818–829. <https://doi.org/10.1016/j.conbuildmat.2017.08.104>
- Lu, X., Teng, J. G., Ye, L., & Jiang, J. J. (2005). Bond-slip models for FRP sheets/plates bonded to concrete. *Engineering Structures*, 27(6), 920–937. <https://doi.org/10.1016/j.engstruct.2005.01.014>
- Massou, M., Babu, N., & Xian, G. (2023). Experimental study on the mechanical properties of CFRP/epoxy composite plates under seawater immersion. *Structures*, 54, 48–57. <https://doi.org/10.1016/j.jistruc.2023.05.042>
- Mofrad, M. H., Mostofinejad, D., & Hosseini, A. (2019). A generic non-linear bond-slip model for CFRP composites bonded to concrete substrate using EBR and EBROG techniques. *Composite Structures*, 220, 31–44. <https://doi.org/10.1016/j.compstruct.2019.03.063>
- Moghaddas, A., Mostofinejad, D., Saljoughian, A., & Iliia, E. (2021). An empirical FRP-concrete bond-slip model for externally-bonded reinforcement on grooves. *Construction and Building Materials*, 281, 122575. <https://doi.org/10.1016/j.conbuildmat.2021.122575>
- Mostofinejad, D., & Mahmoudabadi, E. (2010). Grooving as alternative method of surface preparation to postpone debonding of FRP laminates in concrete beams. *Composite Construction*, 14(6), 804–811. [https://doi.org/10.1061/\(ASCE\)CC.1943-5614.0000117](https://doi.org/10.1061/(ASCE)CC.1943-5614.0000117)
- Mostofinejad, D., Mofrad, M. H., & Hosseini, A. (2018). Investigating the effects of concrete compressive strength, CFRP thickness and groove depth on CFRP-concrete bond strength of EBROG joints. *Construction and Building Materials*, 189, 323–337. <https://doi.org/10.1016/j.conbuildmat.2018.08.203>
- Mostofinejad, D., & Shamel, S. M. (2013). Externally bonded reinforcement in grooves (EBRIG) technique to postpone debonding of FRP sheets in strengthened concrete beams. *Construction and Building Materials*, 38, 751–758. <https://doi.org/10.1016/j.conbuildmat.2012.09.030>
- Reza, Z. G., & Davood, M. (2022). Behaviour of EBRIG CFRP sheet-concrete joint: Comparative assessment with EBR and EBROG methods. *Construction and Building Materials*, 346(5), 128374. <https://doi.org/10.1016/j.conbuildmat.2022.128374>
- Riyam, J., Mohammed, A. M., & Ali, A. S. (2021). Flexural behavior of reinforced concrete beams strengthened by carbon fiber reinforced polymer using different strengthening techniques. *Advances in Structural Engineering*, 25(2), 355–373. <https://doi.org/10.1177/13694332211049992>
- Shaofei, J., Rongbin, Z., & Hualin, S. (2023). Test on shear behavior of surface slotted carbon fiber sheet and concrete interface. *Journal of Harbin Institute of Technology*, 55(06), 52–60.
- Sun, W., Peng, X., & Yu, Y. (2017). Development of a simplified bond model used for simulating FRP strips bonded to concrete. *Composite Structures*, 171, 462–472. <https://doi.org/10.1016/j.compstruct.2017.03.066>
- Tatar, J., & Milev, S. (2021). Durability of externally bonded fiber-reinforced polymer composites in concrete structures: A critical review. *Polymers*, 13(765), 1–24. <https://doi.org/10.3390/polym13050765>
- Teng, J. G., & Smith, S. T. (2002). FRP strengthened RC structures. I: review of debonding strength models. *Engineering Structures*, 24(4), 385–395. [https://doi.org/10.1016/S0141-0296\(01\)00105-5](https://doi.org/10.1016/S0141-0296(01)00105-5)
- Teng, J. G., Smith, S. T., Yao, J., & Chen, J. F. (2003). Intermediate crack-induced debonding in RC beams and slabs. *Construction and Building Materials*, 17(6–7), 447–462. [https://doi.org/10.1016/S0950-0618\(03\)00043-6](https://doi.org/10.1016/S0950-0618(03)00043-6)
- Teng, J. G., Yuan, H., & Chen, J. F. (2006). FRP-to-concrete interfaces between two adjacent cracks: Theoretical model for debonding failure. *International Journal of Solids and Structures*, 43(18), 5750–5778. <https://doi.org/10.1016/j.ijsolstr.2005.07.023>
- Wang, J. (2006a). Debonding of FRP-plated reinforced concrete beam, a bond-slip analysis. I. Theoretical formulation. *International Journal of Solids and Structures*, 43(21), 6649–6664. <https://doi.org/10.1016/j.ijsolstr.2006.01.014>
- Wang, J. (2006b). Cohesive zone model of intermediate crack-induced debonding of FRP-plated concrete beam. *International Journal of Solids and Structures*, 43(21), 6630–6648. <https://doi.org/10.1016/j.ijsolstr.2006.01.013>
- Wang, J. (2007). Cohesive-bridging zone model of FRP-concrete interface debonding. *Engineering Fracture Mechanics*, 74(17), 2643–2658. <https://doi.org/10.1016/j.engframech.2007.02.013>



- Wu, Y. F., Xu, X. S., Sun, J. B., & Jiang, C. (2012). Analytical solution for the bond strength of externally bonded reinforcement. *Composite Structures*, 94(11), 3232–3239. <https://doi.org/10.1016/j.compstruct.2012.04.026>
- Yao, J., Teng, J. G., & Chen, J. F. (2005). Experimental study on FRP-to-concrete bonded joints. *Composite Part B Engineering*, 36(2), 99–113. <https://doi.org/10.1016/j.compositesb.2004.06.001>
- Yuan, C., Chen, W., Pham, T. M., & Hao, H. (2019). Bond behaviour between hybrid fiber reinforced polymer sheets and concrete. *Construction and Building Materials*, 210, 93–110. <https://doi.org/10.1016/j.conbuildmat.2019.03.082>
- Zhang, W. (2018). Prediction of the bond-slip law between externally bonded concrete substrates and CFRP plates under fatigue loading. *International Journal of Civil Engineering*, 16, 1085–1096. <https://doi.org/10.1007/s40999-017-0258-8>
- Zhou, Y. W., Wu, Y. F., & Yun, Y. (2010). Analytical modeling of the bond-slip relationship at FRP-concrete interfaces for adhesively-bonded joints. *Composites, Part b: Engineering*, 41(6), 423–433. <https://doi.org/10.1016/j.compositesb.2010.06.004>
- Zolfaghari, S., Mostofinejad, D., & Fantuzzi, N. (2023). Experimental evaluation of FRP-concrete bond using externally-bonded reinforcement on grooves (EBROG) method. *Composite Structures*, 310, 116693. <https://doi.org/10.1016/j.compstruct.2023.116693>

### Publisher's Note

Springer Nature remains neutral with regard to jurisdictional claims in published maps and institutional affiliations.

**Zehong Han** is now a master degree student at Department of Civil Engineering, Xiamen University, China. He received his bachelor degree of engineering in 2022 in Xiamen University. His research interests include CFRP reinforced structure and bridge engineering.

**Jing Gao** is now a professor at Department of Civil Engineering, Xiamen University, China. She received her ph.d degree of structure engineering in Fuzhou University, China in 2009. Her research interests includes bridge engineering, CFRP application in Civil Engineering structure, and steel-concrete structure.

**Huaihui Song** is now a master degree student in Department of Civil Engineering, Xiamen University, China. He is now focusing on research in the field of CFRP reinforced structure.

**Gongyi Xu** is now a senior engineer in China Railway Bridge Survey and Design Institute Group Co.LTD, Wuhan, China. He has rich experience in suspension bridge design and consultation. He won the John A. Roebling Medal in 2018.